Magnetic moment of thin film superconductors: When thickness matters

C. Pfaff,[1] T. Courtois,[1] M. R. Koblischka,[2] S. Andrieu,[1] J.-X. Lin,[1] M. Hehn,[1] S. Mangin,[1] K. Dumesnil,[1] and T. Hauet[1]

[1]*Université de Lorraine, CNRS, IJL, F-54000, France*

[2]*Saarland University, D-66041 Saarbrücken, Germany*

(Received 27 February 2024; revised 19 August 2024; accepted 23 August 2024; published 5 September 2024)

The evolution of the magnetic moment as a function of the applied magnetic field for a superconducting material is usually described by the so-called Bean model. We show here that this model fails to explain the magnetic response of conventional type-II superconductor films to a field applied perpendicular to the film plane when their thickness is below 100 nm. More precisely, after zero-field cooling below the critical temperature, a positive moment forms in ascending field and an increasing negative moment develops when sweeping the field back to zero. We infer that such an inverted loop behavior in the case of low-thickness films originates from a combination of low pinning, large penetration depth, and large edge demagnetization field. From relaxation experiments, we demonstrate that the magnetic states along the inverted moment versus field loop are stable equilibrium states. Our findings provide some hints to further understand the high-field paramagnetic Meissner effect reported in thin films and prove that field cooling is not required to produce a paramagnetic-like response.

DOI: 10.1103/PhysRevB.110.094502

I. INTRODUCTION

Isothermal diamagnetic response to an external magnetic field (H), due to Meissner currents, is a macroscopic signature of superconductivity. Below their critical temperature (T_c) and above their first critical field (H_{c1}), type-II superconductors host vortices (i.e., normal regions allowing the penetration of a magnetic-flux quantum $\Phi_0 = h/2e$), which reduces the Meissner diamagnetic signal until full cancellation at the second critical field (H_{c2}), where the superconductor turns to normal state. Therefore, the macroscopic magnetic moment (M) of a superconductor is a good probe of the mixed state of type-II superconductor and vortex lattice phases [1,2]. In contrast to this typical diamagnetic response, a paramagnetic response, consecutive to field cooling, from above to below T_c, was also reported in a wide range of superconductors [3–12]. This is commonly referred to as "paramagnetic Meissner effect" (PME), which are of two types. Low-field PME (LFPME) consists of the appearance of a paramagnetic signal whose magnitude is maximum for the smallest cooling-field magnitude in Meissner state from μT to mT range [3,4]. Most often observed in granular bulk superconductors, this phenomenon is explained by an inhomogeneous superconducting transition through an inhomogeneous cooling. A further cooling down then compresses the trapped magnetic flux in the lower-T_c regions and produces a nonequilibrium net paramagnetic moment [5,6]. High-field PME (HFPME) consists of the monotonic increase of the magnetic moment from diamagnetic to paramagnetic as the sample is cooled down in the mixed state under a magnetic field in the range of few millitesla up to few Tesla [7–10]. Contrary to LFPME, the HFPME is more intense for larger fields. For bulk samples, it was speculated that when the temperature is reduced below T_c in the presence of high magnetic fields, flux lines are inhomogeneously trapped and then creep towards pinning centers like dislocations, local variations of alloy concentration, or nonsuperconductive grains [7,9–12]. Similar observations have been also made for 65- and 95-nm-thick Nb films without such inhomogeneous strong pinning centers [8], so that other parameters may also promote HFPME. The impact of the sample shape on HFPME has been confirmed by Geim *et al.* in 2.5-μm-diameter and 100-nm-thick aluminum disks [13]. They demonstrated the presence of an unstable paramagnetic moment under increasing positive magnetic field, which they explained by the nucleation and compression of metastable multivortex state (or a single giant vortex carrying few Φ_0) combined with edge-enhanced penetrating magnetic field due to the demagnetizing field of the thin disk. A deeper understanding of the parameters that influence HFPME would require additional isothermal M vs H measurements for superconducting films with thicknesses below 100 nm, which are extremely rare in the literature.

In the present paper, we report the study of magnetic moment of thin films of various conventional type-II superconductors (MgB_2, NbN, Nb, and V) with thicknesses ranging from 100 down to 5 nm, as a function of applied magnetic field (H) and temperature (T). When H is applied perpendicular to the film plane, superconducting quantum interference device (SQUID) measurements reveal an inverted M vs H loop as compared to typical curves for films thicker than 100 nm or bulk samples. We systematically analyze the influence of film thickness (t) and T on the stability of the observed field-induced paramagnetic-like state and argue that these dependences pinpoint the role of low vortex pinning, geometry-enhanced London penetration length, and thin film edge demagnetization fields. Overall, we demonstrate that HFPME features can be achieved without a field-cooling procedure and that isothermal creep processes explain moment relaxation previously used in the literature to characterize HFPME.

II. EXPERIMENTAL DETAILS

Single-crystal MgB_2 films were deposited by molecular-beam epitaxy (MBE) under ultrahigh vacuum on sapphire (0001) single-crystal substrates. A 5-nm-thick epitaxial MgO (111) buffer layer was deposited prior to MgB_2 in order to allow single-crystal growth of MgB_2 [14]. The substrate temperature was maintained at 370 °C during growth. Mg was evaporated from a Knudsen cell at a 1-Å/s deposition rate while an electron gun was used for the B evaporation at a deposition rate of 0.1 Å/s. A 10-nm-thick capping layer of gold or MgO protected the MgB_2 layer against oxidation. We verified that the capping layer did not influence the magnetometry results (not shown here). The crystalline quality, epitaxial relationships, growth mode, chemical content, and surface flatness were controlled *in situ* by reflection high-energy electron diffraction and x-ray photoemission spectroscopy, as well as *ex situ* by x-ray diffraction and transmission electron microscopy (see Fig. S1 in the Supplemental Material [41]). Note that epitaxial V and epitaxial Nb thin films were also grown by MBE, as well as textured Nb and NbN films with thicknesses ranging from 5 to 30 nm, by sputtering technique on a silicon substrate with a Ta buffer (3 nm) and a Pt capping layer (2 to 3 nm). These samples aimed at proving that the obtained results could be generalized to all type-II superconductors. The magnetic characterizations were performed on $4.5 \times 4.5 - \mathrm{mm}^2$ samples using a commercial Quantum Design SQUID-VSM MPMS3 and PPMS9T mounted with a vibrating-sample magnetometer (VSM) head. A negative linear slope due the diamagnetism of the sapphire substrate was systematically removed from all M vs H loops. The critical temperatures (T_c) of both MBE-grown MgB_2 and sputtered Nb films were deduced from magnetometry data and confirmed by resistance measurements performed on a PPMS9T mounted with an electrical transport rod. T_c values as a function of MgB_2 and Nb film thickness are presented in Fig. S2 [41]. Especially, T_c of MgB_2 only slightly increased from 30.5 to 32.5 K for t ranging from 17 down to 91 nm, and decreased down to zero below 17 nm, in agreement with previous reports [15,16]. Multiple factors could explain the fact that T_c for our films remained lower than the MgB_2 bulk one (39 K) [17]. Between 30 and 90 nm, T_c still slightly increased. By extrapolating this linear increase, 39 K may be reached before 400 nm. We did not investigate such a thick film because of deposition method limits. Samples were capped with Au and thus they underwent a proximity effect which reduced T_c as compared to the intrinsic bulk value. Finally, evaporated and sputtered films on a substrate, and capped with another layer, may carry a larger density of structural defects which can affect the electron mean-free path, and so T_c, as compared to bulk material. Finally, evaporated and sputtered films, on a substrate and capped with another layer, may carry a larger density of structural defects which can affect the electron mean-free path, and so T_c, as compared to bulk material. Using the Ginzburg-Landau equation, we extracted from electrical transport and magnetometry measurements a typical coherence length at 0 K of 4.5 ± 0.5 nm for the MBE-grown MgB_2 films and 12 ± 1 nm for the sputtered Nb films, in good agreement with previous reports [18,19].

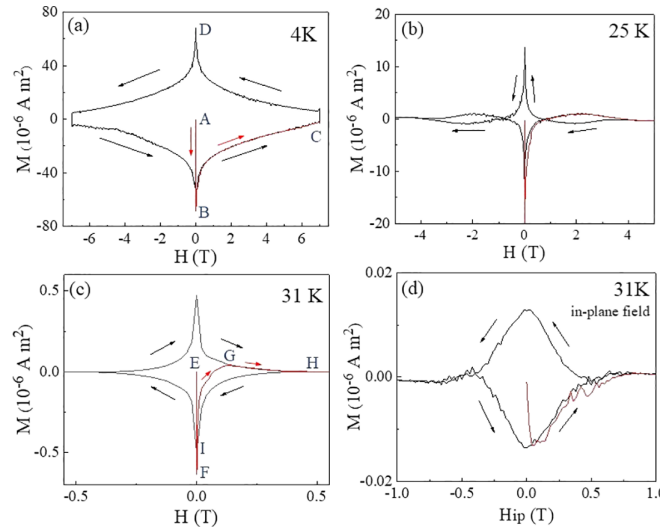

FIG. 1. Magnetic moment (M) of a 91-nm-thick MgB_2 film as a function of the applied magnetic field out of plane for (a)–(c) and in-plane for (d), measured at 4 K (a), 25 K (b), and 31 K (c), (d). The red line is the first magnetization curve, measured immediately after zero-field cooling from above T_c. The black line is the following field loop from +7 to −7 T and back to +7 T. The external magnetic field is swept at 1 mT/s. The arrows indicate the field-sweep direction. Uppercase letters (A–I) are used in the text for description.

III. RESULTS AND DISCUSSION

Figure 1(a) shows the magnetic moment versus out-of-plane magnetic field measured by SQUID-VSM at 4 K for a 91-nm-thick MgB_2 film ($T_c = 32.5$ K). The field-sweeping rate is 1 mT/s. The red curve represents the first magnetization curve following the zero-field cooling (ZFC) procedure from 300 down to 4 K. As expected, $M = 0$ at zero field after ZFC [point A in Fig. 1(a)]. When increasing H, the moment became negative and decreased linearly. This diamagnetic behavior originated from edge Meissner currents that expelled H from the superconducting film [1,2]. The linearity was observed until H reached the so-called penetration field (H_p), here about 1 mT, where positive moments were added to the pure diamagnetic signal [point B in Fig. 1(a)]. These additional positive moments arose from the nucleation of superconducting vortices that allowed H to enter type-II superconductors [2]. Further increase of H led to (i) a densification of the vortices' lattice (depending on the vortex lattice stability and extrinsic features like pinning sites), and (ii) attenuation of the superconductive current due to field-induced depairing of Cooper pairs. As a result, the negative moment magnitude decreased until it reached zero at the so-called second critical field value (H_{c2}), at which the film became a normal metal [2,20]. In Fig. 1(a), H_{c2} was not reached since its value was larger than the maximum field available in our magnetometer (point C). When the field was swept back to lower values, the vortices were partially expelled out of the sample through the edges. When H reached zero [point D in Fig. 1(a)], the positive magnetic moment originated from vortices remained pinned mainly in the center of the sample. From this state, further field cycling provided a symmetric moment versus field loop [21,22]. Figure 1(b) [respectively,

1(c)] shows the measurement sequence for the same sample but performed at 25 K (respectively, 31 K), i.e., temperatures below but close to T_c. Considering the measurement done at 31 K, after ZFC ($M = 0$, point E), an increasing magnetic field applied perpendicularly to the sample film still produced first a diamagnetic moment due to the Meissner effect. Then, when H overpassed H_p (point F at a field lower than 1 mT), the negative moment magnitude decreased due to vortices entering the sample. Nevertheless, instead of reaching zero moment at H_{c2} as at 4 K, the moment crossed first zero value for a field referred to as H_{pos} in the following, then reached a positive maximum value at around 130 mT (point G) before it decreased down to zero at $+H_{c2}$ (point H). Subsequently, when H was reduced from above $+H_{c2}$, the moment became negative and its magnitude monotonically rose until it reached a maximum negative moment for a zero applied field (point I). Further field cycling going to above $-H_{c2}$ provided a symmetric moment versus field loop. Figure 1(b) presents the data obtained with the same procedure at 25 K. The $M(H)$ loop was a mix between the 4 K bulklike behavior, dominant for small applied magnetic fields, and the 31 K inverted behavior, dominant at higher fields. Interestingly, the inverted loops only occurred when the external magnetic field was applied perpendicularly to the superconductive thin film. In Fig. 1(d), moment vs in-plane field loop obtained at 31 K shows bulklike features. Our measurements showed the influence of T, t, and the orientation of the applied field on the paramagnetic phase. In the following, we will analyze these three parameters in greater depth.

In Fig. 2, state diagrams were built for MgB_2 by plotting the crossing field H_{pos} extracted from the first magnetization ramp and H_{c2} as a function of the reduced temperature T/T_c for different thicknesses. In Fig. 2(a) for $t = 91$ nm, below 0.4 T_c, the sample behaved as a typical bulk superconductive sample. Above 0.8 T_c, the *M(H)* loop was fully inverted. And, in between 0.4 T_c and 0.8 T_c, a transition from bulklike to inverted occurred at H_{pos}. We could conclude that both high temperature (below T_c) and high field (below H_{c2}) favored the inverted magnetic state. The aspect ratio of the thin film being a source of discrepancy between films and bulk superconductors and between superconductive states produced by in-plane and out-of-plane external fields [23,24], we analyzed the influence of the film thickness on the inverted regime. Magnetometry measurements were performed on two MgB_2 films with $t = 45$ nm ($T_c = 31.5$ K) in Fig. 2(b) and $t = 15$ nm ($T_c = 20$ K) in Fig. 2(c). For $t = 45$ nm the same general trends and phase diagram as for $t = 91$ nm were observed. However, a pure bulklike *M(H)* loop over the full field range was no longer observed, even for temperatures as low as 0.2 T_c. Additionally, the fully inverted cycle existed over a broader temperature range from T_c down to 0.6 T_c [see zoom-in inset Fig. 2(c)]. These two differences were confirmed and enhanced for the $t = 15$ nm for which only inverted loops were seen for the whole range of tested temperature. In Fig. 2(d), the full inverted loop measured at 4 K for 15-nm-thick film was plotted for comparison with Fig. 1(a) for $t = 91$ nm. At this stage, we could conclude that thin film as well as high temperatures and high magnetic fields promoted inverted M vs H loops. Note that the observations reported here for MgB_2 films were confirmed for other conventional superconductor

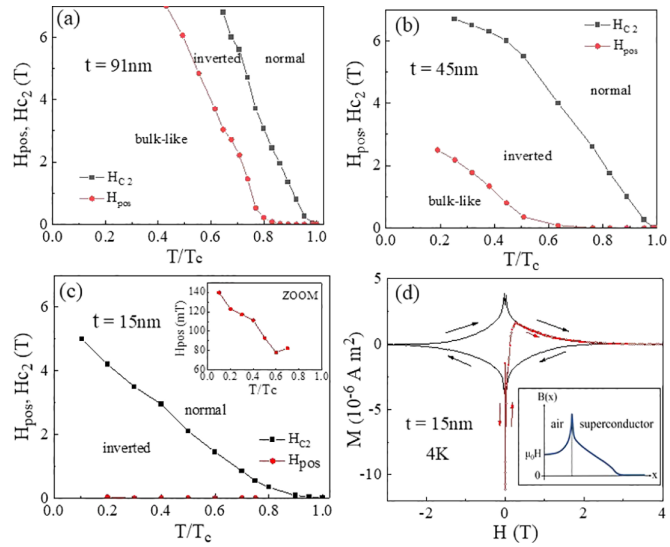

FIG. 2. Critical field H_{c2} (black squares) and transition field H_{pos} (red circles) between negative and positive moment, extracted from the first field ramp after zero-field cooling, as a function of reduced temperature T/T_c for MgB_2 films with thickness $t = 91$ nm (a), $t = 45$ nm (b), and $t = 15$ nm (c). These phase diagrams highlight regions where the films have negative moment (bulklike) and positive moment (inverted). MgB_2 is no longer superconducting in the normal region. The inset in (c) shows a zoom on linear temperature dependence of H_{pos}; (d) magnetic moment of a 15-nm-thick MgB_2 film as a function of out-of-plane magnetic field, measured at $T = 4$ K. The red line is the first magnetization curve, measured immediately after zero-field cooling from above T_c. Inset of (d) is a scheme of the profile of perpendicular induction B as a function of position x near the edge of a thin film superconductor undergoing an increasing magnetic field H applied perpendicularly to the film, as presented in Ref. [26] for instance.

films like epitaxial V, epitaxial Nb, textured Nb, and textured NbN (see Fig. S6 [41]). Figure S3 shows the case of sputtered Nb thin films with thicknesses ranging from 5 to 30 nm [41]. Besides, we verified that the results did not depend on some specific field gradients inside the SQUID magnetometers [6], as demonstrated in Fig. S4 [41].

The stability of the paramagnetic-like state, induced during the first field ramp, was further tested by moment relaxation measurements in a fixed magnetic field for $t = 15$ nm. As shown in Fig. 3(a), after ZFC, under a constant field of 100 mT, the moment relaxed exponentially with a characteristic time (τ) of 540 s towards a positive moment state, while a constant field of 40 mT provided a slower relaxation time of $\tau = 890$ s and smaller relaxation amplitude (see fits in Fig. S5 [41]). Therefore, we could conclude that the processes involved during the first magnetization ramp were activated by H. We performed similar aftereffect experiments from $H > H_{c2}$ down to negative field. In Fig. 3(b), for a low sweeping rate of 1 mT/s, as H decreased from above H_{c2}, a negative moment rose and reached its maximum near zero field. Modifying the field-sweep rate up to 15 mT/s led to a smaller negative, or even positive, moment [red curve in Fig. 3(b)]. When stopping the field sweep at a selected value kept fixed afterwards (at about 0, 100, and 250 mT), M

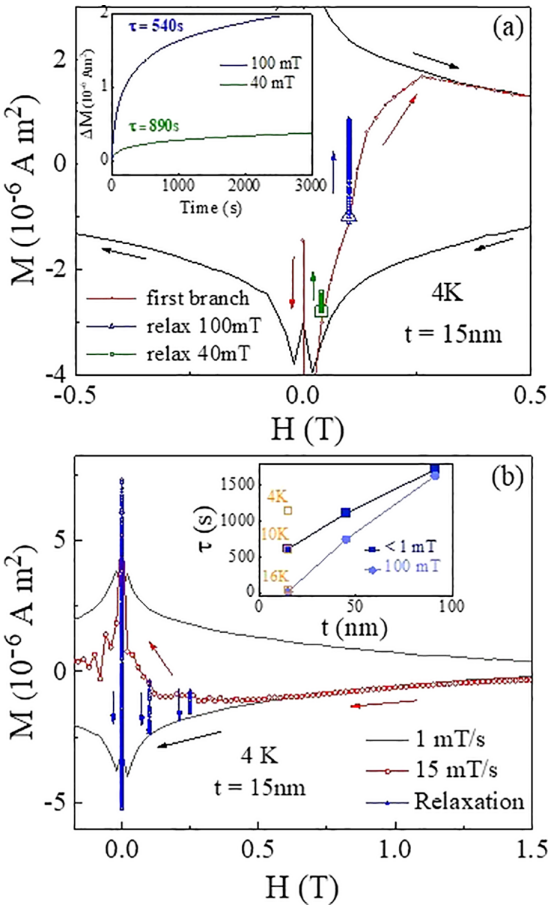

FIG. 3. (a) Full hysteresis loop (black line) and first magnetization curve (red line) measured at 4 K on a MgB_2 (15 nm) film. The blue triangles and the green squares are the measurements of moment vs time under a fixed field of 100 and 40 mT, respectively, after ZFC. In the inset to (a), the same relaxation data are plotted as a function of time. An exponential relaxation is found with relaxation time τ of 540 s for 100 mT and 890 s for 40 mT. (b) Full hysteresis loop measured at 4 K with a field-sweep rate of 1 mT/s (black line) compared to the decreasing field branch from positive field above $+H_{c2}$ to negative field measured with a field-sweep rate of 15 mT/s (red open circles). The blue dots correspond to the moment relaxation in constant field from three points of the red curve, respectively, 250 mT, 100 mT, or near zero field. The moment decrease (see blue arrows) can be fitted by an exponential function with a relaxation characteristic time (τ). In inset to (b), τ values are plotted as a function of film thicknesses, for the same reduced $T/T_c = 0.5$, and for two constant fields, namely 100 mT (light blue disks) and lower than 1 mT (dark-blue filled squares). Three open squares are added to show the acceleration of the relaxation when the temperature rises from 4 to 16 K, for the 15-nm-thick sample near zero field.

relaxed from the red curve down to the main hysteresis loop [black curve in Fig. 3(b)]. This relaxation was exponential and the single relaxation time (τ) decreased, i.e., the relaxation was eased, when temperature and/or fixed-field intensity was raised, and/or when the film thickness was reduced [inset in Fig. 3(b)]. Overall, these relaxation experiments demonstrated that the inverted state (including the positive moment state or paramagnetic-like state in ascending field) was a stable equilibrium state.

Let us now consider how the film thickness can impact the magnetic response of superconductor thin film and lead to a positive moment in ascending field, at the opposite of the usual bulk superconductors diamagnetism. As theoretically studied in detail in Refs. [25] and [26], the large demagnetization factor of thin film produced an enhanced value of the magnetic field in the penetrated region at the sample edge [see inset of Fig. 2(d)]. Its maximum could reach $H_{\text{edge}} = H\sqrt{L/t}$ (with L the typical lateral dimension of the film). In other words, a 15-nm-thick superconductor film with millimetric lateral dimensions experienced, in part of the penetrated region near the edges, a field up to several hundred times larger than H. One direct consequence was that the field required to transit from the Meissner state to the vortex state, i.e., the field required to nucleate the first vortices, was drastically reduced in a thin film as compared to the intrinsic critical field H_{c1}. Indeed, the penetration field H_p for a 15-nm-thick MgB_2 film at 4 K [Fig. 2(d)] was lower than 0.5 mT, whereas $H_{c1}(0) =$ 110 mT was carefully quantified in similar single-crystalline MgB_2 films with several micrometer thickness [27,28]. As already pointed out by Geim *et al.* [13], a second consequence of enhanced magnetic field at the edge was an additional paramagnetic signal to the magnetic moment of the superconductor film. Indeed, the SQUID magnetometer collected the whole magnetic flux located in the sample apart from the homogeneous external field H. A region of the sample where the magnetic field was larger than H translated into a positive moment, as well as a region from which the field was expulsed by Meisner screening resulted in a negative moment. The edge region providing the additional positive magnetic moment in ascending H depended on the field penetration length [26]. In thin film superconductor with thickness smaller than the bulk London penetration length λ, the effective penetration length was no longer λ but $\Lambda = 2\lambda^2/t$ [29–32]. In a 15-nm-thick film, and considering the intrinsic bulk $\lambda(0\text{ K}) \approx 100$ nm for MgB_2 [27,33–35], $\Lambda(0\text{ K})$ overpassed 1 μm. Since both H_{edge} and $\Lambda(0\text{ K})$ increased when the film thickness shrunk, it was expected that the additional positive moment provided by the edge field rose when t what reduced. The fact that Λ increased with the sample temperature according to $\Lambda(T) = \Lambda(0)[1-(T/T_c)^4]^{-1}$ [35] was also consistent with the experimental observation that temperature favored the positive moment in ascending field after ZFC, as well as the overall inverted loop (see Fig. 1).

At that stage, it had to be noted that in real millimetric samples, scratches on the thin film, preexisting at the substrate surface or due to sample handling, often existed and could also be source of additional effective edges. In order to further characterize the influence of the edge-field effects on promoting positive magnetic moment, we performed cuts on a 45-nm-thick MgB_2 film with a diamond saw and successively isolated 4, 8, and finally 12 regions, within the same initial sample area. By doing so, we increased the total edge length relative to the sample surface. As shown in Figs. S7(a)–S7(d), for the full film and then after each cutting step, we measured magnetization versus out-of-plane field, at 16 K after zero-field cooling, similar to the data presented in Fig. 1(b). As shown in Fig. S7(e), H_{pos} decreased when increasing the number of cuts [41]. This meant that the cutting process

favored the "inverted state." It was consistent with a positive moment produced by the sample edges, although one could not exclude that it also partially related to a modification of the vortex nucleation at the new rough artificial edges. Nevertheless, the overall shape of the $M(H)$ loop did not change drastically with the number of cuts. If the enhanced edge field was the leading mechanism promoting the inverted $M(H)$ loop, one would have expected to have a much more significant evolution towards a full inverted loop. This was not the case.

The contribution of edge-enhanced field to the positive moment was not enough to obtain a positive moment in the Meissner state since the volume diamagnetic moment was much larger. Nevertheless, the field-induced introduction of vortices, above H_p, lowered the volume diamagnetic signal and eventually allowed a positive moment for a field larger than H_{pos}. As shown in Fig. S8 [41], the moment variation around H_{pos} was quite "reversible" as long as it did not visit a significant portion of the main hysteresis loop. Moreover, our relaxation experiments in Fig. 3 confirmed that the vortex propagation was a field-activated and thermally activated process. H_{pos} decreased linearly with temperature. Vortex mobility was also affected by the film thickness since a larger density of defects was expected in thicker films, and so H_{pos} rose with the film thickness. The large vortex mobility, gained in increasing the field, increasing the temperature, and lowering the film thickness, must produce a decrease of the critical current J_c [3,36–38]. Therefore, one could expect a consequent decrease of the diamagnetic signal magnitude while preserving a significant positive moment signal from the vortices. This, coupled to the positive moment from the enhanced edge field, may lead to an overall positive moment.

The decrease of moment at high field up to H_{c2}, common to both the first magnetization curve after ZFC and the full hysteresis loop [see for instance Fig. 2(d)], could be explained by two complementary effects: (i) the increasing external field allowed vortices to penetrate the whole sample area and densified the vortex lattice; thus, the enhancement of the edge field was continuously reduced since the difference between the field inside and outside the sample was gradually suppressed, and (ii) the Cooper pair density, and so the critical current in the superconducting regions of the sample continuously decreased when the external field increased up to H_{c2} due to orbital effect [20,39]. For a 15-nm-thick film, decreasing H from H_{c2} led to a negative moment whose magnitude reached a maximum at zero field [Fig. 2(d)]. Such behavior has already been observed in superconductors when the vortices were expulsed in a reversible manner in the absence of strong volume pinning centers [40]. Usually, as observed in Figs. 2(a) and 2(b) for our thickest film, below a certain field, the pinning was strong enough to conserve pinned vortices in the center of the sample and to generate a remanent positive moment as in any bulk type-II superconductor. It was no longer the case for the thinnest film [Fig. 2(d)] since a reduced film thickness gives rise to a lower density of defects, as well as a stronger vortex-vortex repulsion due to the enhanced vortex extension $2\Lambda(T)$ [29]. Note that in the descending branch from H_{c2}, an additional negative moment must have been provided by the edge field since the positive field magnitude inside the superconductive sample remained larger than the external field H. See the Supplemental Material [41].

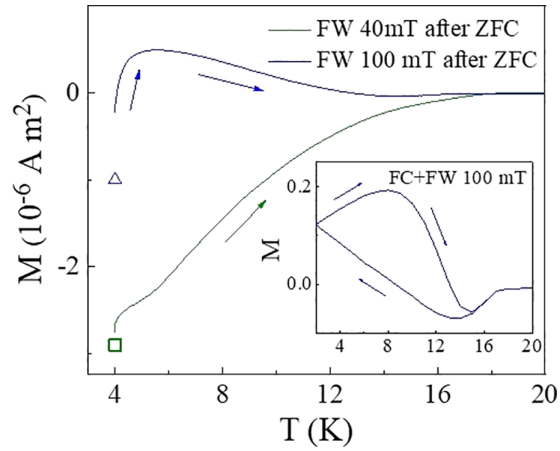

FIG. 4. Magnetic moment (M) as a function of temperature (T) measured on a MgB_2 (15 nm) film during warming under fixed field (FW) of 100 mT (blue line) and 40 mT (green line), after ZFC. The two symbols indicate the same two starting points as in the relaxation experiments plotted in Fig. 3(a). The inset shows the moment measured during field cooling (FC) at 100 mT from 25 down to 2 K, and then field warming (FW) in 100 mT from 2 to 25 K.

Finally, it was interesting to compare the isothermal relaxation process that we obtained as function of time in a fixed applied field in Fig. 3(a) with the one reported as a function of temperature in the case of HFPME in the literature [8,9]. In Fig. 4, after ZFC down to 4 K, H was raised up to either 40 or 100 mT. Then, under fixed field, the moment was measured during a temperature cycle from 4 up to 24 K (i.e., above T_c). The single green open square and single blue open triangle corresponded to ones in Fig. 3(a), at 40 and 100 mT, respectively, before relaxation. In Fig. 4, when the temperature rose, an increase of the moment up to positive value was observed, followed by a shallower decrease, consistently with previous data obtained for Nb films [8]. This first increase of moment was similar to the isothermal relaxation described in the inset of Fig. 3(a) under 100 mT. As a matter of fact, the time required to perform the $M(T)$ measurement from 4 to 20 K was typically of the order of 1000 s. Note that similar relaxation features were seen both for $M(T)$ measurements performed after ZFC or FC in 100 mT (inset to Fig. 4) accordingly with Ref. [8]. Using a 40-mT fixed field after ZFC, instead of 100 mT, only allowed the vortex state to slightly relax and a significant negative moment remained. So, we concluded that in thin enough films, the increase of moment during $M(T)$ that led to the so-called HFPME in Ref. [8] had the same origin as the one observed here during $M(H)$ after ZFC (Fig. 3) and, therefore, that such HFPME feature did not necessarily require a field-cooling procedure.

IV. SUMMARY

In conclusion, we studied the M vs H loops of various conventional type-II superconductor films with thicknesses ranging from 100 down to 5 nm. The out-of-plane field hysteresis loops for the thinnest films were inverted compared

to the one usually observed for bulk superconductor and described by Bean's model. In particular, after ZFC, the magnetic moment reached a positive value when increasing the field. When decreasing the external field from above H_{c2} down to zero, the moment was negative and its magnitude increased with decreasing field, which led to a negative moment at remanence. From relaxation experiments, we demonstrated that the mixed states adopted along the inverted loop were stable equilibrium states, contrary to previous reports on micrometer-wide disks [13]. We correlated the field, temperature, and thickness dependence of these inverted loops to the large penetration length, the vortex mobility, and the edge demagnetization fields which are specific features of thin films. Finally, our observations showed that high-field paramagnetic Meissner effect (HFPME) [8] could be achieved during isothermal field sweep or by vortex relaxation under fixed field in the absence of any field-cooling procedure.

ACKNOWLEDGMENTS

The authors thank B. Leridon, A. Silhanek, and N. Lejeune for fruitful discussions. The authors gratefully acknowledge the CC-3M at Institut Jean Lamour for the transmission electron microscopy images of MgB_2 films, especially S. Migot, J. Ghanbaja, and M. Emo. The work was supported by the "SONOMA" project cofunded by FEDER-FSE Lorraine et Massif des Vosges 2014–2020, a European Union Program, and by the French National Research Agency through the France 2030 Government Grant No. PEPR SPIN ANR-22-EXSP 0008.

[1] C. P. Poole Jr., H. A. Farach, and R. J. Creswick, *Superconductivity* (Academic Press, New York, 1995).

[2] P. Mangin and R. Kahn, *Superconductivity: An Introduction* (Springer International Publishing AG, 2017).

[3] M. R. Koblischka, L. Pust, C. S. Chang, T. Hauet, and A. Koblischka-Veneva, The paramagnetic Meissner effect (PME) in metallic superconductors, Metals **13**, 1140 (2023).

[4] M. S. Li, Paramagnetic Meissner effect and related dynamical phenomena, Phys. Rep. **376**, 133 (2003).

[5] A. E. Koshelev and A. I. Larkin, Paramagnetic moment in field-cooled superconducting plates: Paramagnetic Meissner effect, Phys. Rev. B **52**, 13559 (1995).

[6] P. Kostic, B. Veal, A. P. Paulikas, U. Welp, V. R. Todt, C. Gu, U. Geiser, J. M. Williams, K. D. Carlson, and R. A. Klemm, Paramagnetic Meissner effect in Nb, Phys. Rev. B **53**, 791 (1996).

[7] A. I. Rykov, S. Tajima, and F. V. Kusmartsev, High-field paramagnetic effect in large crystals of $YBa_2Cu_3O_{7-\delta}$, Phys. Rev. B **55**, 8557 (1997).

[8] A. Terentiev, D. B. Watkins, L. E. De Long, D. J. Morgan, and J. B. Ketterson, Paramagnetic relaxation and Wohlleben effect in field-cooled Nb thin films, Phys. Rev. B **60**, R761 (1999).

[9] F. T. Dias, P. Pureur, P. Rodrigues, Jr., and X. Obradors, Paramagnetic effect at low and high magnetic fields in melt-textured $YBa_2Cu_3O_{7-\delta}$, Phys. Rev. B **70**, 224519 (2004).

[10] S. K. Ramjan, L. S. Sharath Chandra, R. Singh, and M. K. Chattopadhyay, Strong paramagnetic response in the superconducting state of Y-containing $V_{0.6}Ti_{0.4}$ alloys, Supercond. Sci. Technol. **35**, 105006 (2022).

[11] S. Sundar, M. K. Chattopadhyay, L. S. S. Chandra, and S. B. Roy, High field paramagnetic Meissner effect in $Mo_{100-x}Re_x$ alloy superconductors, Supercond. Sci. Technol. **28**, 075011 (2015).

[12] M. Matin, M. K. Chattopadhyay, L. S. S. Chandra, and S. B. Roy, High-field paramagnetic Meissner effect and flux creep in low-T_c Ti–V alloy superconductors, Supercond. Sci. Technol. **29**, 025003 (2016).

[13] A. K. Geim, S. V. Dubonos, J. G. S. Lok, M. Henini, and J. C. Maan, Paramagnetic Meissner effect in small superconductors, Nature (London) **396**, 144 (1998).

[14] L. Li, H. Zhang, Y.-H. Yang, and G.-X. Miao, High-quality epitaxial MgB_2 Josephson junctions grown by molecular beam epitaxy, Adv. Eng. Mater. **19**, 1600792 (2017).

[15] C. Zhang, Y. Wang, D. Wang, Y. Zhang, Z.-H. Liu, Q.-R. Feng, and Z.-Z. Gan, Suppression of superconductivity in epitaxial MgB_2 ultrathin films, J. Appl. Phys. **114**, 023903 (2013).

[16] M. Naito and K. Ueda, MgB_2 thin films for superconducting electronics, Supercond. Sci. Technol. **17**, R1 (2004).

[17] W. N. Kang, H.-J. Kim, Eun-Mi Choi, C. U. Jung, and S.-I. Lee, MgB_2 superconducting thin films with a transition temperature of 39 kelvin, Science **292**, 1521 (2001).

[18] S. Patnaik, L. D. Cooley, A. Gurevich, A. A. Polyanskii, J. Jiang, X. Y. Cai, A. A. Squitieri, M. T. Naus, M. K. Lee, and J. H. Choi, Electronic anisotropy, magnetic field-temperature phase diagram and their dependence on resistivity in *c*-axis oriented MgB_2 thin films, Supercond. Sci. Technol. **14**, 315 (2001).

[19] P. Quarterman, N. Satchell, B. J. Kirby, R. Loloee, G. Burnell, N. O. Birge, and J. A. Borchers, Distortions to the penetration depth and coherence length of superconductor/normal-metal superlattices, Phys. Rev. Mater **4**, 074801 (2020).

[20] D. V. Shantsev, Y. M. Galperin, and T. H. Johansen, Thin superconducting disk with field-dependent critical current: Magnetization and ac susceptibilities, Phys. Rev. B **61**, 9699 (2000).

[21] C. P. Bean, Magnetization of hard superconductors, Phys. Rev. Lett. **8**, 250 (1962).

[22] D.-X. Chen and R. B. Goldfarb, Kim model for magnetization of type-II superconductors, J. Appl. Phys. **66**, 2489 (1989).

[23] F. E. Harper and M. Tinkham, The mixed state in superconducting thin films, Phys. Rev. **172**, 441 (1968).

[24] M. Tinkham, *Introduction to Superconductivity* (McGraw-Hill, New York, 1996).

[25] E. Zeldov, J. R. Clem, M. McElfresh, and M. Darwin, Magnetization and transport currents in thin superconducting films, Phys. Rev. B **49**, 9802 (1994).

[26] E. H. Brandt, Theory of type-II superconductors with finite London penetration depth, Phys. Rev. B **64**, 024505 (2001).

[27] L. Lyard, T. Klein, J. Marcus, R. Brusetti, C. Marcenat, M. Konczykowski, V. Mosser, K. H. Kim, B. W. Kang, H. S. Lee,

and S. I. Lee, Geometrical barriers and lower critical field in MgB_2 single crystals, Phys. Rev. B **70**, 180504(R) (2004).

[28] B. Kang, H.-J. Kim, M.-S. Park, K.-H. Kim, and S.-I. Lee, Reversible magnetization of MgB_2 single crystals with a two-gap nature, Phys. Rev. B **69**, 144514 (2004).

[29] J. Pearl, Current distribution in superconducting films carrying quantized fluxoids, Appl. Phys. Lett. **5**, 65 (1964).

[30] J. R. Clem, Two-dimensional vortices in a stack of thin superconducting films: A model for high-temperature superconducting multilayers, Phys. Rev. B **43**, 7837 (1991).

[31] L. Embon, Y. Anahory, Ž. L. Jelić, E. O. Lachman, Y. Myasoedov, M. E. Huber, G. P. Mikitik, A. V. Silhanek, M. V. Milošević, A. Gurevich, and E. Zeldov, Imaging of super-fast dynamics and flow instabilities of superconducting vortices, Nat. Commun. **8**, 85 (2017).

[32] L. Ceccarelli, D. Vasyukov, M. Wyss, G. Romagnoli, N. Rossi, L. Moser, and M. Poggio, Imaging pinning and expulsion of individual superconducting vortices in amorphous MoSi thin films, Phys. Rev. B **100**, 104504 (2019).

[33] C. Buzea and T. Yamashita, Review of superconducting properties of MgB_2, Supercond. Sci. Technol. **14**, R115 (2001).

[34] D. K. Finnemore, J. E. Osbenson, S. L. Bud'ko, G. Lapertot, and P. C. Canfield, Thermodynamic and transport properties of superconducting $Mg^{10}B_2$, Phys. Rev. Lett. **86**, 2420 (2001).

[35] T. Nishio, S. Okayasu, J.-i. Suzuki, N. Kokubo, and K. Kadowaki, Observation of an extended magnetic field penetration in amorphous superconducting MoGe films, Phys. Rev. B **77**, 052503 (2008).

[36] C. J. van der Beek, M. Konczykowski, A. Abal'oshev, I. Abal'osheva, P. Gierlowski, S. J. Lewandowski, M. V. Indenbom, and S. Barbanera, Strong pinning in high-temperature superconducting films, Phys. Rev. B **66**, 024523 (2002).

[37] T. Shapoval, H. Stopfel, S. Haindl, J. Engelmann, D. S. Inosov, B. Holzapfel, V. Neu, and L. Schultz, Quantitative assessment of pinning forces and magnetic penetration depth in NbN thin films from complementary magnetic force microscopy and transport measurements, Phys. Rev. B **83**, 214517 (2011).

[38] C. J. van Der Beek, Flux pinning, in *Handbook of Superconductivity*, 2nd ed., edited by D. A. Cardwell, D. C. Larbalestier, and A. Braginski (CRC Press, Boca Raton, 2022).

[39] E. H. Brandt, Superconductor disks and cylinders in an axial magnetic field. I. Flux penetration and magnetization curves, Phys. Rev. B **58**, 6506 (1998).

[40] J. D. Livingston, Magnetic properties of superconducting lead-base alloys, Phys. Rev. **129**, 1943 (1963).

[41] See Supplemental Material at http://link.aps.org/supplemental/10.1103/PhysRevB.110.094502 for additional figures supporting the claims of main text.